



The effect of repeated alkali pretreatments on the morphological characteristics of cellulose from oil palm empty fruit bunch fiber-reinforced epoxy adhesive composite

Romi Sukmawan^{a,*}, Kusmono^b, Anugrah Perdana Rahmanta^c, Lestari Hetalesi Saputri^c

^a Department of Mechanical Technology, Politeknik Lembaga Pendidikan Perkebunan, Jl. LPP 1 A, Balapan, Yogyakarta, 11840, Indonesia

^b Department of Mechanical and Industrial Engineering, Faculty of Engineering, Universitas Gadjah Mada, Jl. Grafika No. 2, Yogyakarta, 55281, Indonesia

^c Department of Chemical Technology, Politeknik Lembaga Pendidikan Perkebunan, Jl. LPP 1 A, Balapan, Yogyakarta, 11840, Indonesia

ARTICLE INFO

Keywords:

Resin-based composites
Surface morphology
Mechanical properties of adhesives
Environmental issue
OPEFB
Alkali treatment

ABSTRACT

In this study, the effect of low-concentration (4 wt%) alkali and bleaching pre-treatments on the fibrillation of oil palm empty fruit bunch (OPEFB) fibers were evaluated. The OPEFB fibers were subjected to repeated weak alkali treatment and bleached by hydrogen peroxide in alkaline solution. Fibrillation was accomplished via mechanical process by a household blender. The obtained cellulose morphology was used to find paper-like sheets that were coated with epoxy resin to produce composites by sheet lamination. Fourier-transform infrared spectroscopy revealed that hemicellulose and lignin were partially removed and fiber dispersion strongly depended on the number of alkali treatment cycles. Scanning electron microscopy showed that fibers that underwent 12 alkali treatment cycles presented the most effective fibrillation. In addition, the blender fibrillation of cellulose fibers in a mild (6 wt%) alkali solution required less energy than blending in a neutral aqueous medium and improved fibrillation into nanofibrils. The obtained average diameters of the microfibrils and nanofibrils were approximately 7 μm and 89 nm, respectively. The tensile strength and Young's modulus of the composites were approximately 3.6 and 20 times higher, respectively, than those of neat epoxy resin. The proposed chemo-mechanical method could facilitate the use of micro-nanofibrils extracted from OPEFB for fiber-based materials and polymeric composites.

1. Introduction

Nowadays, owing to the increasing interest in environmentally friendly materials and technologies, inexpensive and eco-friendly fibers with high specific strength are widely used to reinforce resin, which, in turn, is used to transfer the load to the reinforcing fibers. Such fiber-resin composites are easily degradable; therefore, their impact on the environment is negligible. Oil palm empty fruit bunches (OPEFB), which are a type of natural fiber, have been increasingly used to manufacture reinforced composites [1]. In 2019, Indonesia, which is one of the world's largest palm oil producers, produced 43 million tons of crude palm oil from 11.75 million planted hectares [2] and generated 47.3 million tons of OPEFB as biomass waste. As OPEFB fibers are rich in cellulose (42–65% by mass) [1], they are potential raw materials for producing cellulose fiber as reinforcement for polymer resin composites.

A series of chemical treatments are typically required to remove

lignin and hemicellulose from lignocellulosic materials before mechanical disintegration. For example, the (2,2,6,6-tetramethylpiperidin-1-yl) oxidanyl (TEMPO)-mediated oxidation of cellulose has been used to introduce negatively charged (e.g., carboxyl or carboxymethyl) groups on cellulosic fibers, improve their subsequent fibrillation, and significantly decrease the energy input required for mechanical disintegration [3,4]. Carboxymethylation is another pretreatment that increases the number of anionic charges during the process, which confers a high charge to fibrils, and facilitates their fibrillation [5]. However, the high cost of such pretreatments can limit their use. Acidified sodium chlorite has been widely used for cellulose delignification and extraction from wood or non-wood materials [6–9]. Chlorite ions (ClO_2^-) can produce chlorine radicals ($\text{Cl}\cdot$), which further react with lignocellulosic materials and fragment them into many harmful chemicals (highly toxic organochlorines). The alkali pretreatment is more environmentally friendly and economical than other chemical methods [10]. The alkali

* Corresponding author.

E-mail address: rms@polteklpp.ac.id (R. Sukmawan).

pretreatment involves the use of sodium hydroxide (NaOH), lime, ammonia, or alkaline hydrogen peroxide (AHP) [11–13]. Among alkali pretreatment agents, NaOH and hydrogen peroxide (H_2O_2) are extensively used to treat lignocellulosic materials before disintegration. Cai et al. investigated the effect of weak (5 wt%) and strong (10 and 15 wt%) alkali treatment on the mechanical properties of abaca fibers and revealed that alkali treatment gradually removed hemicelluloses and lignin from abaca fibers, causing the separation of abaca fiber bundles into individual elementary fibers and cell wall swelling [14]. The Young's modulus of fibers subjected to weak (5 wt%) alkali pretreatment was 41% higher, whereas the Young's moduli of fibers subjected to strong alkali pretreatment (10 and 15 wt%) were 24% and 29% lower, respectively, than that of untreated fibers [14]. Scatolino et al. fractionated lignin and hemicellulose from wood species and reported that the residual lignin and hemicellulose content after 4 wt% alkali pretreatment followed by bleaching with 24% H_2O_2 was low [15,16]. Several researchers have contributed to the development of the AHP pretreatment for enhanced enzymatic hydrolysis for different types of biomasses [11]. After pretreatment, biomass is typically subjected to a multi-step process, including successive refining, enzymatic hydrolysis, carboxymethylation, or quaternization, followed by homogenization, TEMPO-mediated oxidation, and mechanical disintegration via blending or homogenization or high-intensity ultrasonication [17]. The combination of chemical and mechanical disintegration using high-speed blenders has been increasingly used because of its low energy consumption and mass production suitability [8,9,18]. Recently, our team has combined NaOH and H_2O_2 hydrolysis and successfully extracted cellulose micro-nanofibrils from bagasse using a household blender [13, 19]. The results showed that a combination of chemo-mechanical treatment using a household blender positively affected mechanical fibrillation. The diameter of the obtained fibers varied between 20 nm and 20 μm .

Several researchers have investigated the effect of alkali and AHP solution concentrations on the morphology and mechanical properties of OPEFB fibers and their amenability to manufacturing reinforced composites using thermosetting and thermoplastic resins, such as epoxy and polypropylene resins [20–22]. However, the poor compatibility between the greater quantity of hydrophilic fibers and hydrophobic resins (epoxy and polypropylene) becomes the main disadvantage of natural fibers in composites.

Utani and Yano (2011) [9] have conducted a comprehensive study investigating the nanofibrillation mechanisms of fibers using a blender. However, the effect of repeated pretreatment on the degree of fibrillation of fibers has not been studied yet.

In this study, a combination of chemo-mechanical treatments has been considered for modifying fiber surface morphologies for improving the mechanical properties of cellulose-based natural fibers as reinforced epoxy adhesive resin composites.

Cellulose micro-nanofibrils were obtained via mechanical fibrillation using a household blender. The properties of the treated cellulose fibers were analyzed using scanning electron microscopy (SEM), Fourier-transform infrared (FTIR) spectroscopy, and X-ray diffraction (XRD) analyses. The proposed eco-friendly pretreatment method can be useful for partial deconstruction of OPEFB microfibrils to nanofibrils. The nanofibrils present on the microfibrils surface can serve as self-reinforcement for improving mechanical properties and compatibility with thermosetting adhesive resins (epoxy).

2. Materials and methods

2.1. Materials

OPEFB were supplied by PT Perkebunan Nusantara VIII Cikarang Bogor, West Java, Indonesia. Analytical grade NaOH and H_2O_2 (Merck, EMD Milipore Corp., Germany) were used as purchased. UHU quick set epoxy adhesive, which was used to fabricate OPEFB cellulose sheet

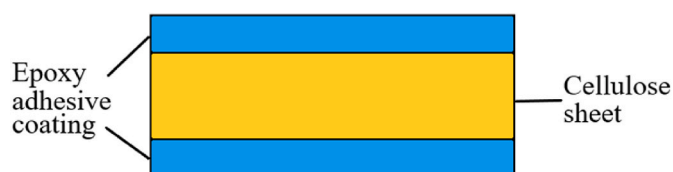


Fig. 1. Schematic illustration of epoxy adhesive resin coating arrangement on the cellulose sheet surface.

composites, was acquired from a local store. A HR2096 (Phillips) 800 W and 21 000 rpm household blender was used for mechanical fibrillation.

2.2. OPEFB fiber treatment

2.2.1. Fiber pretreatment

Untreated cellulose fibers were ground (30 mesh) and subsequently pretreated with NaOH and H_2O_2 , as follows.

- (i) Four weak alkali pretreatment cycles were followed by H_2O_2 bleaching. Raw OPEFB fibers were immersed in a 4 wt% aqueous solution of NaOH four times, and the treated pulp fibers were subjected to bleaching twice using a 5 wt% aqueous solution of H_2O_2 under alkaline conditions (a NaOH solution was added to the H_2O_2 solution until the pH reached 11) to fabricate cellulose.
- (ii) Eight weak alkali pretreatment cycles were followed by H_2O_2 bleaching. This pretreatment was similar to (i) but the alkali pretreatment was repeated eight times.
- (iii) Twelve weak alkali pretreatment cycles were followed by H_2O_2 bleaching. This pretreatment was similar to (i) but the alkali pretreatment was repeated 12 times.

Alkali pretreatment was performed at 75 °C under constant agitation for 45 min, and the NaOH solution-to-OPEFB weight ratio was 20:1. Bleaching was performed at 80 °C under constant agitation for 60 min, and the H_2O_2 solution-to-pulp fiber weight ratio was 40:1. Lastly, the isolated cellulose was washed several times with distilled water until a pH of ~ 7 was attained to remove the residual NaOH from the cellulose.

2.2.2. Fibrillation process

Cellulose was fibrillated by a household blender. Cellulose samples (0.5 g) that underwent pretreatments (i), (ii), and (iii) were added to 500 mL of water and blended using the blender at 21 000 rpm for 10 min [13,19]. The prepared samples were denoted as 4SB, 8SB, and 12SB, respectively. For comparison, a cellulose sample that underwent pretreatment (iii) was blended in a mild (6 wt%) alkali solution to evaluate the effect of alkali concentration on blending. The prepared sample denoted as 12SB6.

2.3. Composite preparation

The 4SB, 8SB, and 12SB samples were vacuum filtered using a Whatman filter with 2.5 μm pores to obtain wet cellulose sheets. Each wet sheet was placed between metal wire nets and filter paper and dried at 65 °C for 1 h to produce sheets with a thickness of $\sim 40 \mu\text{m}$ and a diameter of $\sim 8 \text{ cm}$. Ribbon-shaped samples (80 mm \times 10 mm) were cut from the sheets and epoxy adhesive was coated onto their surfaces as shown in Fig. 1. The sheet-to-adhesive weight ratio was 3:7. Lastly, the samples were conditioned in an oven at 60 °C for 30 min to produce a thin-skin composite with a thickness of $\sim 0.5 \text{ mm}$. The composites fabricated using the 4SB, 8SB, and 12SB sheets were denoted 4SR, 8SR, and 12SR, respectively.

2.4. SEM and EDX analysis

The morphology of the OPEFB fibers before and after the chemo-

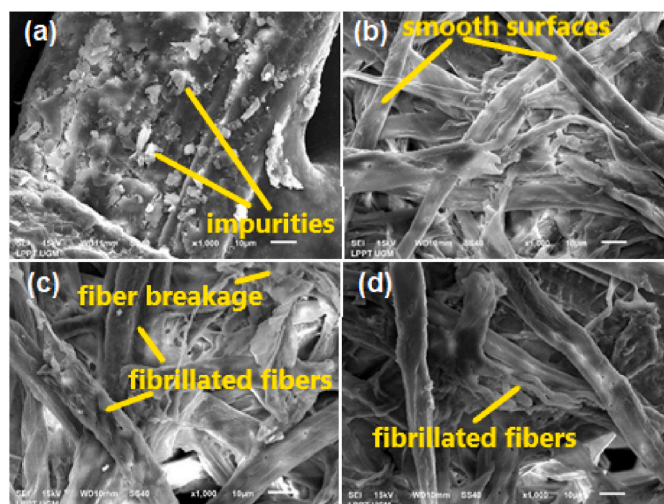


Fig. 2. SEM images of (a) raw OPEFB fibers and cellulose fibers fabricated from OPEFB fibers subjected to (b) 4, (c) 8, and (d) 12 pretreatment cycles with a 4 wt% aqueous solution of NaOH followed by blending.

mechanical treatment was observed using a SEM instrument (JSM-6510LA, JEOL Ltd.). The samples were placed on carbon tapes and coated with a thin Au layer using a sputter coater (JEC-3000 FC, JEOL Ltd.). The SEM instrument was equipped with an EDX device, which was used to determine the elemental composition (wt.%) of each sample.

2.5. Image analysis

The cellulose fiber diameter distribution after chemo-mechanical treatment was determined using the ImageJ freeware (National Institute of Health, USA) for image analysis. Approximately 50 representative fibers from the SEM images of the samples were analyzed and plotted as fiber diameter range function.

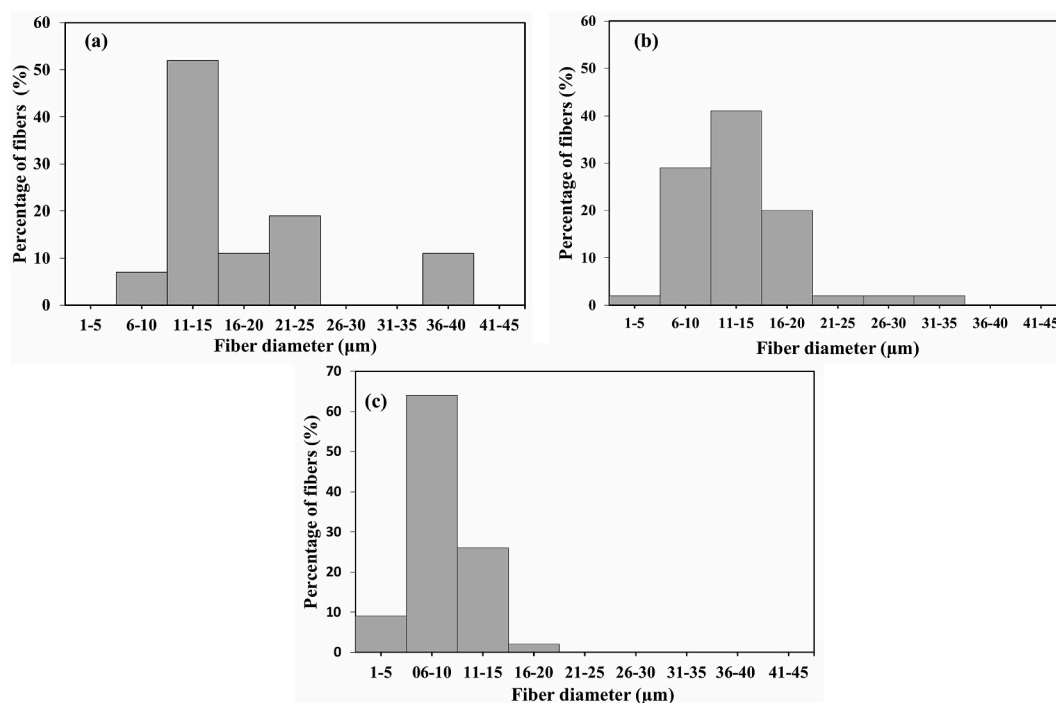


Fig. 3. Diameter distribution of cellulose fibers fabricated from oil palm empty fruit bunch fibers subjected to (a) 4, (b) 8, and (c) 12 pretreatment cycles with a 4 wt% aqueous solution of NaOH followed by blending.

2.6. FTIR spectroscopy

The functional group composition of the untreated and chemo-mechanically treated cellulose fibers was determined by dispersing powdered fiber samples in KBr pellets (OPEFB fiber: KBr = 1:50 (w/w)) using a FTIR spectrometer (Nicolet iS10, Thermo Fisher Scientific). The FTIR spectrum of each sample was recorded in transmittance mode in the wavenumber range of 4000–800 cm^{-1} using 32 scans at a resolution of 8 cm^{-1} .

2.7. XRD

The crystalline structure of untreated and chemo-mechanically treated cellulose fibers was examined using an XRD system (LabX XRD-6100, Shimadzu) with Cu K α radiation ($\lambda = 1.5406 \text{ \AA}$) at 40 kV and 30 mA in the 2θ range of 3° – 30° , with a scan step of 0.02° , and at a scanning rate of $1.5^\circ/\text{min}$. The crystallinity indices (CIs) of the samples were calculated according to the Hermans method [23,24], as follows:

$$CI = A_{\text{cryst}}/A_{\text{total}} \quad (1)$$

where A_{cryst} is the sum of the crystalline band areas, and A_{total} is the total area under the XRD patterns. The crystallite size (CS) of each sample (in nm) was calculated using the Scherrer method [23], as follows:

$$CS = (K \lambda)/(\beta \cos \theta) \quad (2)$$

where CS (nm) is the crystallite size in the direction perpendicular to the (200) lattice plane, K (0.89) is a constant that depends on the crystal shape, λ is the wavelength of the (200) plane ($\lambda = 1.5425 \text{ \AA}$), β (rad) is the peak width at half-maximum height of the incident X-ray, and θ is the Bragg angle of the (200) reflection.

2.8. Tensile testing

The tensile strength and modulus of neat epoxy adhesive (resin) and micro-nanofibrillated cellulose sheet filled epoxy composites were measured through a universal testing machine (HT-9501 Electro-

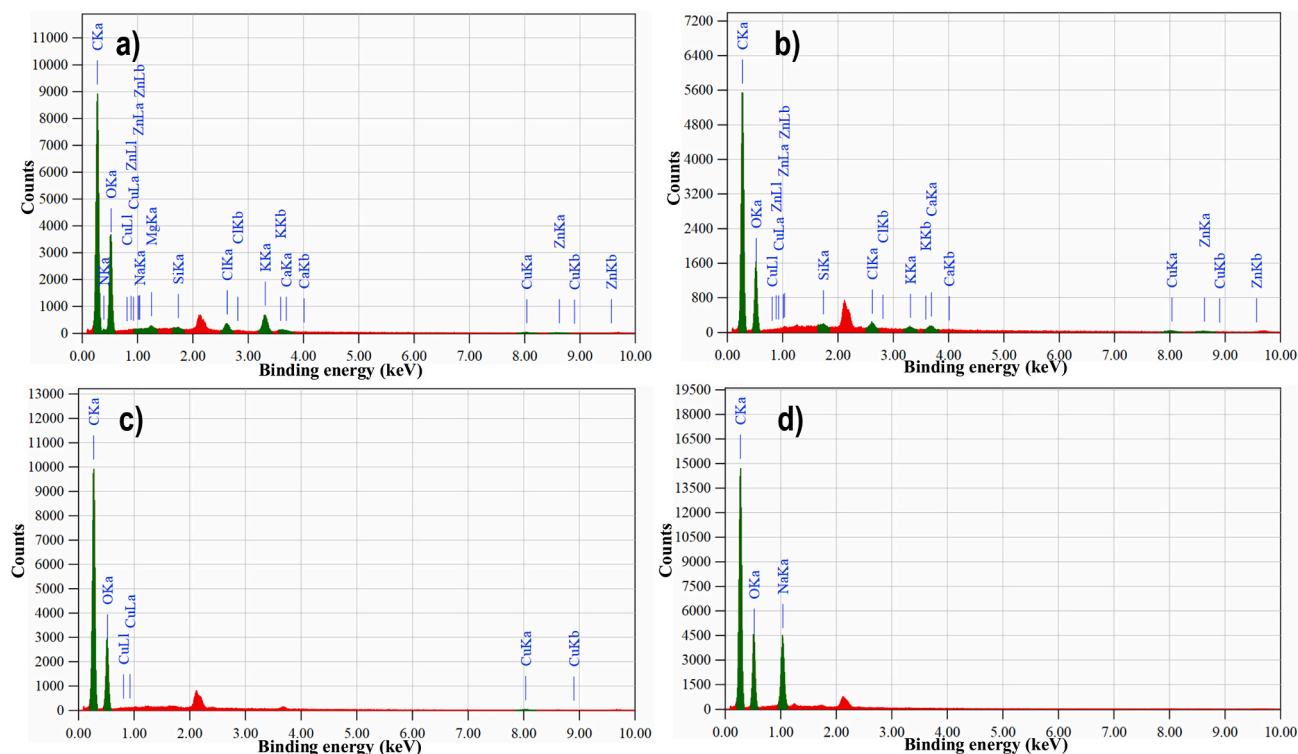


Fig. 4. Elemental composition of (a) raw oil palm empty fruit bunch (OPEFB) fibers and cellulose fibers fabricated from OPEFB fibers subjected to (b) 4, (c) 8, and (d) 12 pretreatment cycles with a 4 wt% aqueous solution of NaOH followed by blending determined using energy-dispersive X-ray spectroscopy.

Hydraulic Servo). All the sample preparation was carried out as per specifications of ASTM D 882. A standard head displacement at a speed of 12.5 mm/min was applied. For each type of sample, five replicate specimens were tested and average results of tensile strength and modulus were calculated.

3. Results and discussion

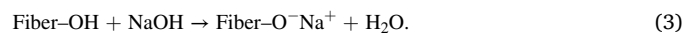
3.1. SEM–EDX analysis

The SEM images of the untreated OPEFB fibers and after chemo-mechanical treatment are illustrated in Fig. 2(a)–(d). The raw fibers were covered with many impurities (Fig. 2(a)). However, after chemo-mechanical treatments, all fibers presented smooth surfaces (Fig. 2(b)–(d)), suggesting that almost all impurities were removed. The 8SB sample presented a relatively wide fiber diameter range (Fig. 2(b)), which was attributed to the continuous removal of amorphous lignin and hemicelluloses from the cellulose fiber surface after chemo-mechanical treatment contributing to fiber swelling, fibrillation, and breaking.

The fiber diameters of all samples were manually measured by counting image pixels using the Image J processing software. The average diameter of the raw fibers was relatively uniform ($130 \pm 26 \mu\text{m}$). For the treated fibers, approximately 50 representative fibers from the SEM images of the 4SB, 8SB, 12SB, and 12SB6 samples were analyzed, and the percentage of fibers with the same diameter was plotted as a function of the fiber diameter range (Fig. 3). It was found that the average diameter of the 4SB, 8SB, and 12SB samples were 18 ± 9 , 13 ± 6 , and $9 \pm 3 \mu\text{m}$, respectively (Fig. 3(a)–(c)). The smallest diameter was exhibited by the 12SB sample subjected to twelve cycles of alkali treatment. This indicated that the diameter of the cellulose fibers was decreased with increasing the number of alkali pretreatment cycles. The increase in alkaline treatment cycle caused a large amount of dissolved amorphous components which further resulted in a smaller diameter. The obtained average diameter of the cellulose fibers shown

by the 12SB sample ($9 \mu\text{m}$) was lower compared to previous results reported by Kassab et al. [25] which produced the cellulose microfibrils (CMF) with an average diameter of $20 \mu\text{m}$. The resulting difference in diameter was attributed to the different sources of cellulose and pretreatment conditions. It was well-documented that the dimensions of cellulose fibers is strongly influenced by the cellulose sources and pretreatment conditions [26,27].

The elemental compositions of the raw, 4SB, 8SB, and 12SB samples determined using SEM and EDX analyses are presented in Fig. 4. OPEFB fibers mainly consist of cellulose, lignin, hemicelluloses, and waxes [1]. The EDX spectrum of the OPEFB fibers (Fig. 4(a)) includes peaks corresponding to the binding energies of C, O, and several inorganic elements, such as Zn, Cu, Ca, K, Cl, Si, Mg, and Na. The raw, 4SB, 8SB, and 12SB samples contained 44.10%, 62.31%, 62.54%, and 70% of C, respectively, and 34.94%, 34.97%, 32.01%, and 27.21% of O, respectively, as the major components (Fig. 4(b)–(d)). The percentages of the organic N and almost all inorganic elements decreased significantly after the OPEFB samples underwent several chemo-mechanical cycles. However, Na impurities were present in the outer layer of the fibers after several NaOH pretreatment cycles (Fig. 4(d)). This could be attributed to the bonds formed and changes that occurred at the surface of the OPEFB fibers during repeated NaOH pretreatment cycles. The reaction between NaOH and OPEFB fibers can be described as follows:



The EDX analysis results revealed that the increase in C content of the fibers that underwent chemo-mechanical treatment can be attributed to the treatment removing a fraction of inorganic elements and N, which increased fiber purity. Moreover, the decrease in O content can be attributed to the effect of the alkali pretreatment cycles, which led to the decrease in the number of hydrophilic hydroxyl groups on the surface of the treated fibers [28]. However, many other factors can contribute to the changes in internal structure and surface morphology of the fibers that affected the C and O contents of the fibers, such as hemicellulose and lignin components.

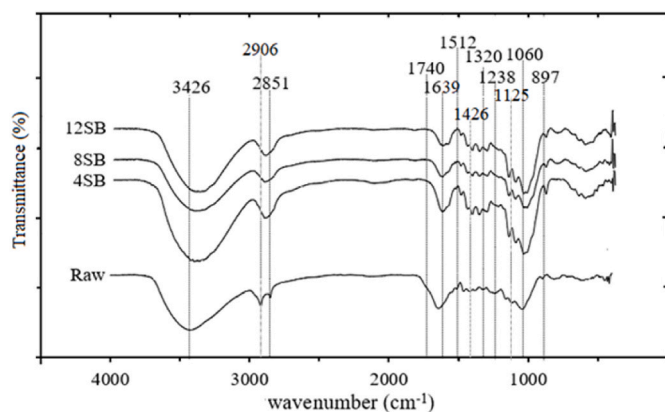


Fig. 5. Fourier-transform infrared spectra of untreated oil palm empty fruit bunch (OPEFB) fibers (raw) and cellulose fibers fabricated from OPEFB fibers subjected to 4, 8, and 12 pretreatment cycles with a 4 wt% aqueous solution of NaOH followed by blending (4SB, 8SB, and 12 SB, respectively).

Table 1

Intensities of Fourier-transform infrared spectra peaks of raw oil palm empty fruit bunch (OPEFB) and cellulose fibers fabricated from OPEFB fibers subjected to 4, 8, and 12 pretreatment cycles with a 4 wt% aqueous solution of NaOH followed by blending (4SB, 8SB, and 12 SB, respectively).

Wavenumber (cm ⁻¹)	Raw	4SB	8SB	12SB
2851	0.7115	–	–	–
1639	1.0857	0.8211	0.7619	0.6254
1320	0.4515	0.8316	0.7227	0.8245
1238	0.5637	–	–	–
1125	0.8810	0.8316	0.7227	0.8245
897	0.1088	0.3530	0.3331	0.3059

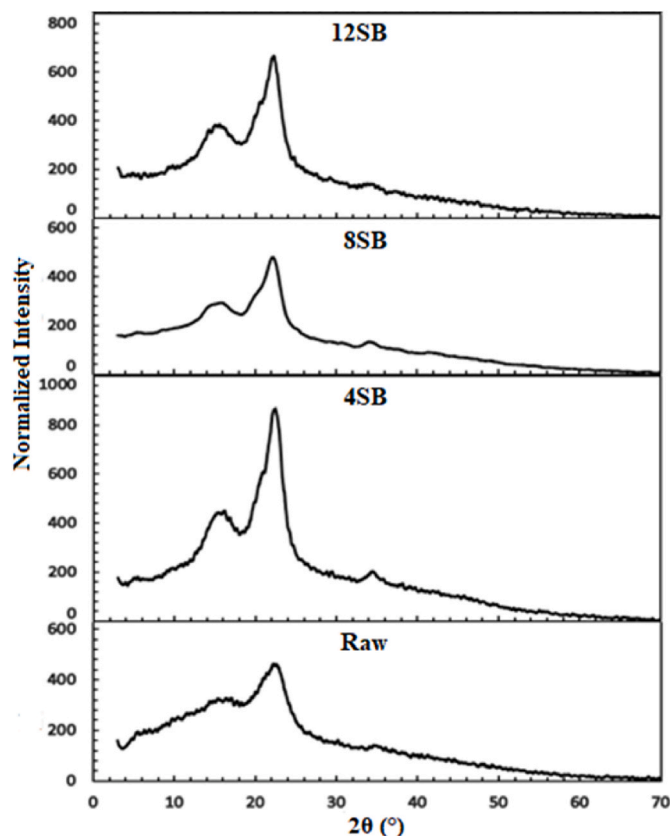


Fig. 7. X-ray diffractogram of raw oil palm empty fruit bunch (OPEFB) and cellulose fibers fabricated from OPEFB fibers subjected to 4, 8, and 12 pretreatment cycles with a 4 wt% aqueous solution of NaOH followed by blending (4SB, 8SB, and 12 SB, respectively).

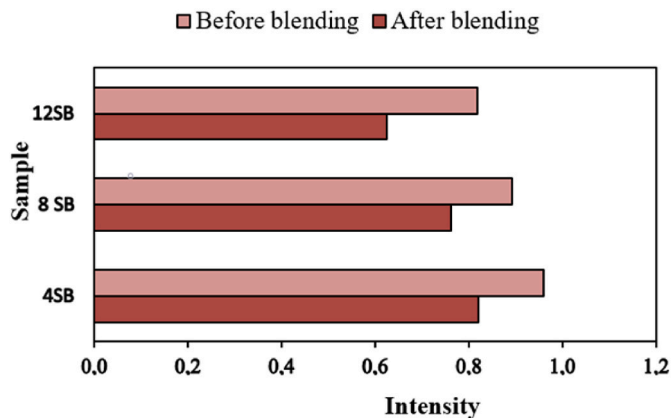


Fig. 6. The intensities of Fourier-transform infrared spectra peaks of lignin (1639 cm⁻¹) comparison between before and after blending in different pretreatments.

3.2. FTIR analysis

The changes in chemical composition of the fibers due to chemo-mechanical treatments were evaluated via FTIR spectroscopy. The FTIR spectra of the raw and treated fibers is shown in Fig. 5. Two main transmittance regions at low (500–1800 cm⁻¹) and high wavenumbers (2700–3500 cm⁻¹) were observed in the FTIR spectra of all samples, and the results were in agreement with the data reported by Saba et al. [29]. The transmittance peaks of the raw OPEFB fibers at 3400, 2906, 1320, and 1150–1050 cm⁻¹ were attributed to the stretching vibrations of the –OH groups, C–H groups, H–C–H rings, and C–O groups of cellulose, respectively; the peaks at 2851 and 897 cm⁻¹ were attributed to the

stretching and rocking vibrations, respectively, of the C–H groups of cellulose [30,31]; the peak at 1238 cm⁻¹ was ascribed to the stretching of the C–C groups of hemicellulose; and the peaks at 1639 and ~1512 cm⁻¹ corresponded to the stretching of the C=O and C=C bonds of the aromatic ring of lignin [32]. The intensities of the aforementioned peaks decreased after pretreatment owing to the partial degradation of hemicellulose and lignin, as previously confirmed using chemical analyses (Table 1).

The peaks at 2851 and 1238 cm⁻¹ disappeared after chemo-mechanical treatment owing to the chemo-mechanical treatment degrading hemicellulose and lignin [33]. These results were further supported by the decrease in intensity of the characteristic lignin peak at 1639 cm⁻¹ after chemo-mechanical treatment (Table 1). This decrease in intensity was ascribed to the combination of alkali pretreatment blending cycles (mechanical disintegration) causing lignin solubilization. The effect of mechanical disintegration on the decreasing of lignin during the treatment was supported by the decrease of lignin intensity as shown in Fig. 6. On the other hand, the blending provided a turbulent flow of the fiber suspension, which may have increased the probability of fibers colliding with the blades. Consequently, chemo-mechanical treatment improved fiber fibrillation. The absorption peak at 1426 cm⁻¹ was assigned to amorphous and crystalline cellulose I [34]. The peak at 1426 cm⁻¹ shifted to 1461 cm⁻¹ (characteristic of crystallized cellulose), indicating that the chemo-mechanical treatment partially removed the amorphous fraction of the OPEFB fibers and improved the crystallinity of the fabricated cellulose fibers. The intensity of the peak at 897 cm⁻¹ in the FTIR spectrum of 12SB was lower than those of the same peak in the FTIR spectra of 8SB and 4SB, indicating that the number of NaOH pretreatment cycles partially degraded the amorphous fraction of cellulose (Table 1). The intensities of the cellulose peak at

Table 2

Crystallinity indices (CIs) and crystallite sizes (CSs) along the (200) crystallographic plane of raw oil palm empty fruit bunch (OPEFB) and cellulose fibers fabricated from OPEFB fibers subjected to 4, 8, and 12 pretreatment cycles with a 4 wt% aqueous solution of NaOH followed by blending (4SB, 8SB, and 12SB, respectively).

Sample	CI (%)	CS (nm)
raw	26	2.79
4SB	42.5	3.94
8SB	29.41	3.71
12SB	33.33	4.02

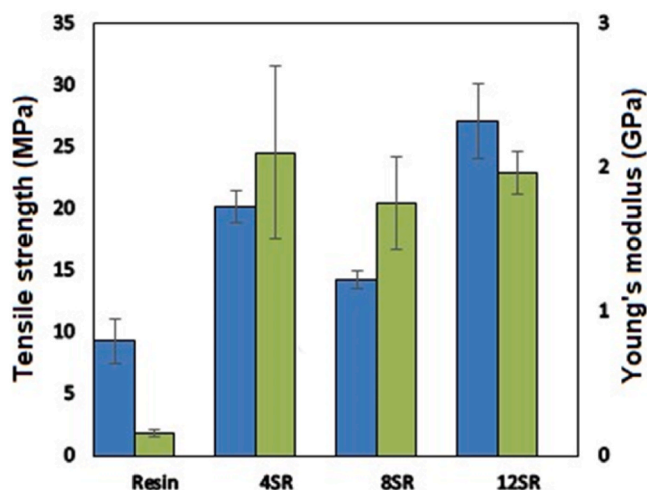


Fig. 8. Tensile strength and the Young's modulus of neat epoxy adhesive resin, and composites based on cellulose fibers fabricated from oil palm empty fruit bunch fibers subjected to 4, 8, and 12 pretreatment cycles with a 4 wt% aqueous solution of NaOH followed by blending (4SR, 8SR, and 12SR, respectively).

1320 and 1125 cm^{-1} increased after pretreatment (Table 1). However, the intensities of the peaks tended to decrease with the number of alkali pretreatment cycles owing to the decrease in intramolecular hydrogen bonding strength with the number of alkali pretreatment cycles [35].

3.3. XRD analysis

The XRD profiles of the raw OPEFB and chemo-mechanically treated fibers are presented in Fig. 7. After deconvolution, all diffractograms included peaks in the 2θ ranges of 14.5–15.3°, 15.7–16.30°, 18.30–18.40°, and 21.90–22.20°, which were assigned to the (1–10) crystallographic plane, the (110) crystallographic plane, amorphous phase, and the (200) crystallographic plane of cellulose I, respectively, and a peak at $2\theta = 35^\circ$, which was ascribed to the (004) crystallographic plane of cellulose I [14,23,36]. The CIs of the raw OPEFB and chemo-mechanically treated fibers were determined using the Hermes equation (Eq. (1)). The CIs of the chemo-mechanically treated fibers were different and were higher than that of the raw OPEFB fibers (Table 2). The CI increased with increasing CS because the crystallite surface was associated with the decrease in inaccessible surface/amorphous cellulose fraction [37]. The average CSs of the raw OPEFB, 4SB, 8SB, and 12SB samples were determined to be 2.79, 3.94, 3.71, and 4.02 nm, respectively, using the Scherrer equation (Eq. (2)). These values were similar to those reported for crystalline cellulose nanoparticles obtained from wood pulp using a high-speed blender [9].

The CI and CS values of the 8SB sample were lower than those of the 4SB sample which may be due to the amorphous lignin and hemicelluloses surrounding semicrystalline cellulose being partially extracted during the chemo-mechanical treatment [14] and also because fibers

swelled, defibrillated, and broke after blending [9] (Fig. 2). However, as some amorphous components and a fraction of amorphous cellulose were removed, the XRD peaks characteristic of the crystalline regions became more prominent [38]. The CI and CS of the 12SB sample were higher than those of the 8SB sample. Overall, the XRD results suggested that the crystallinity of the cellulose fibers in this study was increased via alkali pretreatment followed by blending.

3.4. Mechanical performance of composite fibers

The mechanical strength and Young's modulus of the neat epoxy adhesive resin and one-ply laminate composites are presented in Fig. 8. The tensile strengths and Young's moduli of the composites were higher than those of the neat resin. The tensile strengths of the neat resin, 4SR, 8SR, and 12SR were 9.3, 20.1, 14.2, and 27.1 MPa, respectively. Therefore, the tensile strength of the 12SR composite was approximately three times higher than that of the neat resin. The increase in the number of alkali pretreatment cycles contributed to the decrease in diameter or increase in surface area of the microfibrils, which led to the increase in the number of groups that could form hydrogen bonds between microfibrils and between the microfibrils and resin [39]. However, the tensile strength of 8SR was lower than that of the 4SR sample even though the average diameter of the 8SB sample fibers was smaller than that of the 4SB sample fibers. This can be attributed to microfibrils fibrillating and breaking, which prevented them from effectively reinforcing the epoxy resin. These results were in agreement with the SEM and XRD data.

The Young's moduli of the neat resin, 4SR, 8SR, and 12SR were 0.2, 2.1, 1.8, and 2.0 GPa, respectively. The Young's moduli of the composites did not change significantly with the number of alkali pretreatment cycles and were approximately 10 times higher than that of the neat epoxy adhesive resin. However, if we consider the standard deviation, the Young's modulus of 12SR was lower than those of 8SR and 4SR. This was attributed to the regularities in dispersion and diameter distribution of the 12SB sample compared to those of the 8SB and 4SB samples. In addition, owing to the higher dissolution of lignin and hemicellulose fractions after 12 alkali pretreatment cycles (12SB), the intrafibrillar regions of the 12SB sample were less dense and rigid than those of the 4SB and 8SB samples, allowing the microfibrils to rearrange along the tensile deformation direction and strengthening their tensile characteristics [40,41].

3.4.1. Blending using a mild alkali solution

To improve fiber fibrillation, the probability of fibers colliding with the blender blades should be increased. We achieved this by blending the cellulose fibers in a mild alkali solution, which caused cell wall swelling [14] and increased the probability of swelled fibers colliding with the blender blades. Blending cellulose in a mild (6 wt%) alkali solution after 12 cycles of weak alkali pretreatment contributed to partial fibrillation of microfibrils to nanofibrils, (Fig. 9(a) and (b)). This was ascribed to the continuous removal of residual lignin and hemicellulose during the alkali pretreatment cycles facilitating fiber swelling, which contributed to the increase in probability of fibers colliding with the blender blades and led to increasing fibrillation of microfibrils to nanofibrils.

Cellulose swelling is an intricate process. Studies regarding NaOH treatment of cellulose fibers revealed that the diameter of Na^+ ions (0.276 nm) was favorable for widening and penetrating the smallest pores between the lattice planes of cellulose molecules [12]. The $-\text{OH}$ groups of cellulose were converted to $-\text{ONa}$ groups, increasing the size of cellulose molecules [42]. Consequently, NaOH treatment increased the amount of swollen cellulose molecules in fiber cell walls. Defibrillated nanofibrils can be observed on the surfaces of the microfibrils in the SEM image in Fig. 9(b). The nanofibrils on the surface of microfibrils can serve as self-reinforcement for microfibrils during composite fabrication. Additionally, a good microfibril dispersion can contribute to a good nanofibril distribution in cellulose sheets and composites. The average

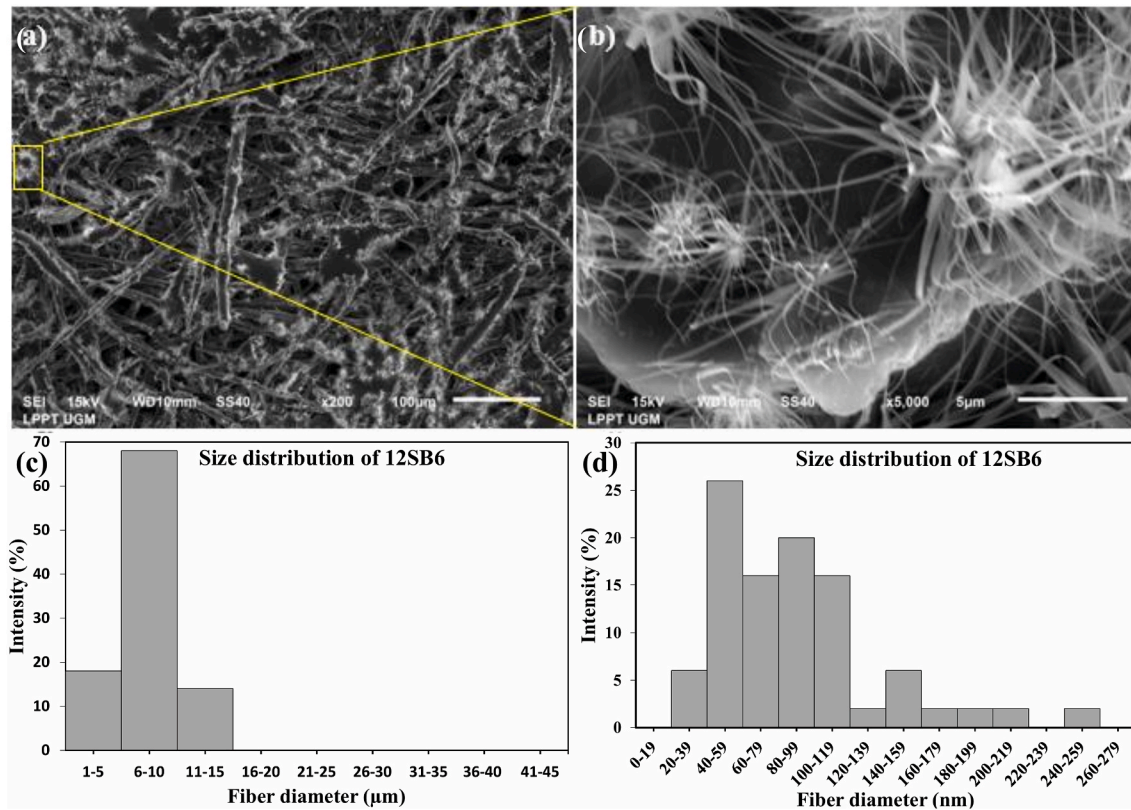


Fig. 9. Morphology analysis. Scanning electron micrographs of (a) and (b) cellulose fibers fabricated from oil palm empty fruit bunch (OPEFB) fibers subjected to 12 pretreatment cycles with a 4 wt% aqueous solution of NaOH followed by blending in a mild (6 wt%) alkali solution (12SB6) at different magnifications. Diameter distribution of 12SB6 (c) microfibers and (d) nanofibrils.

Table 3

Tensile strengths and Young’s moduli of composites prepared by reinforcing cellulose sheets fabricated from oil palm empty fruit bunch fibers subjected to 12 pretreatment cycles with a 4 wt% aqueous solution of NaOH followed by blending in water (12SR) and in a mild (6 wt%) alkali solution (12SR6) solutions with epoxy adhesive resin.

Sample	Tensile strength ^a (MPa)	Young’s modulus ^a (GPa)
12SR	27.1(3.0)	2.0(0.2)
12SR6	33.0(0.1)	3.9(0.2)

^a The values in parentheses are standard deviations.

fiber diameter of the 12SB6 sample was smaller than that of the 12SB sample under the same pretreatment conditions (Fig. 9(c) and (d)). The cell walls of the fibers in the 12SB6 sample were deconstructed and

presented several entangled micro-nanofibrils. The microfiber and nanofibril diameters of the 12SB6 sample were $7 \pm 2 \mu\text{m}$ and $86 \pm 46 \text{ nm}$, respectively. The diameter and width distribution of the micro-nanofibrils of the 12SB6 sample were smaller and narrower, respectively, than those of the 12SB sample. This suggested that blending cellulose fibers under mild alkali conditions (12SB6) required less energy for fibrillation than blending in an aqueous solution (12SB). Blending fibers in a mild alkali solution could facilitate fibrillation because the fibers swelled in the alkali solution. Approximately 68% of the 12SB6 samples consisted of microfibers with a diameter in the range of 6–10 μm and nanofibrils with a diameter lower than 100 nm. The value of the diameter of micro-nano fiber (12SB6) was at a comparable level with the micro-nano fiber during mechanical treatments following high-speed homogenization obtained by Dilamian and Noroozi et al. [43]. Nanofibrils with a diameter lower than 100 nm can serve as fillers

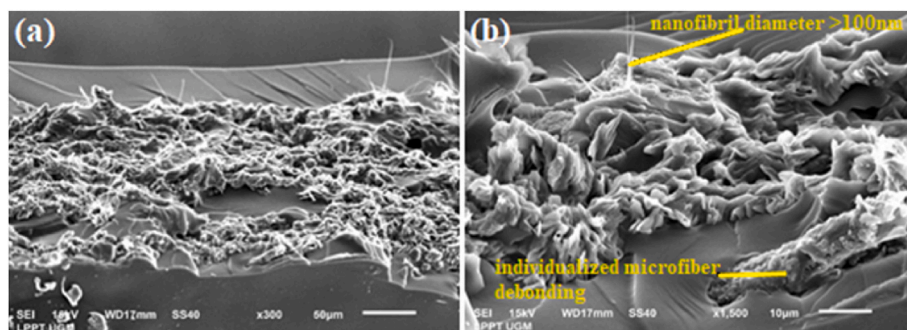


Fig. 10. (a) Scanning electron micrographs of the fracture surface of the composite with a fiber content of 30 wt% prepared by reinforcing cellulose sheets fabricated from OPEFB fibers subjected to 12 pretreatment cycles with a 4 wt% aqueous solution of NaOH followed by blending in a mild (6 wt%) alkali solution and (b) magnified micrograph of the fibers.

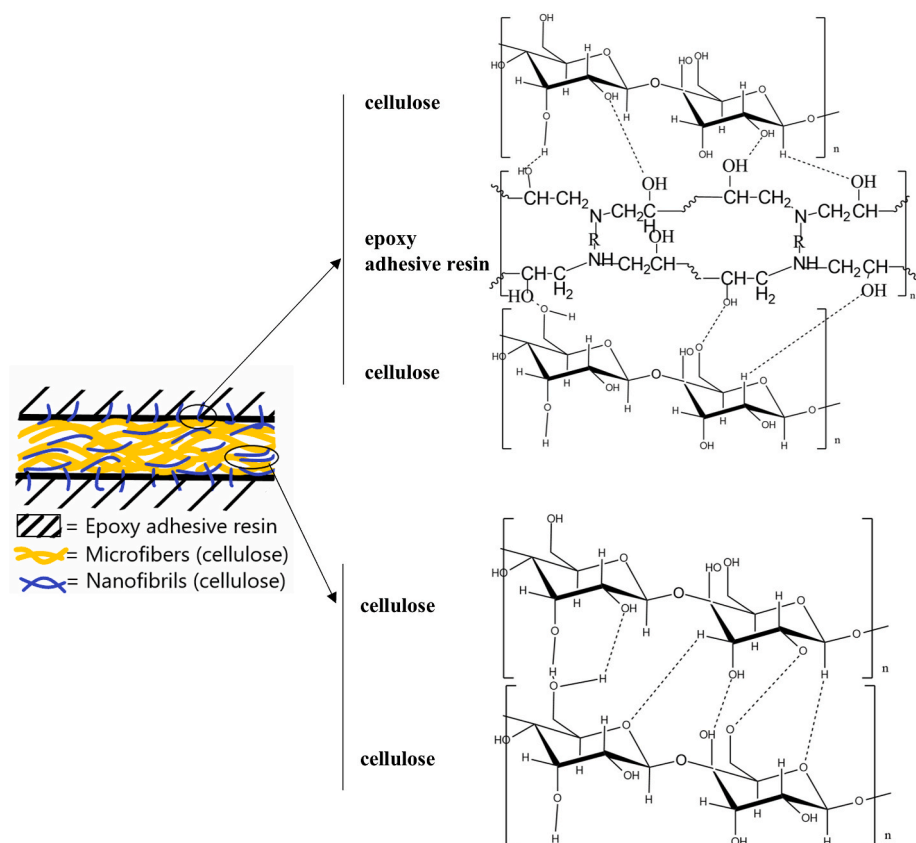


Fig. 11. Schematic diagram of possible interactions between the epoxy adhesive resin, cellulose microfibrils, and cellulose nanofibrils.

or reinforcements in composites [44]. To fabricate reinforced composites based on cellulose sheets, a wider diameter distribution can reduce sheet strength, whereas a narrow diameter distribution can improve strength.

The tensile strength and Young's modulus of the 12SR6 composite, which was prepared by reinforcing a 12SB6 sample with epoxy adhesive resin, was higher than that of 12SR owing to the presence of nanofibrils, which increased the effective surface area available for contact between fibers and the strength of the interfacial hydrogen bonds between fibers and the resin (Table 3).

Cellulose fibers protruded from resin at the fracture surface (Fig. 10 (a)). The protruding fibers were relatively short. Moreover, the SEM image of the fracture surface of 12SR6 revealed that resin penetration into the regions around the fibers in the cellulose sheet can facilitate the contact between resin and cellulose fibers (Fig. 10(a)) [12]. These observations confirmed the good adhesion between resin and cellulose. However, individual microfibrils and nanofibrils debonded from resin and the cellulose sheet, respectively (Fig. 10(b)). The remaining thicker microfibrils or nanofibrils with incompletely fibrillated morphologies and residual Na impurities from the alkali pretreatment cycles on the fiber surfaces can act as defects and can lower composite strength.

Cellulose fibers are more hydrophilic, and the epoxy adhesive resin is more hydrophobic. However, even if the epoxy resin is relatively hydrophobic, the $-C-O-C-$ epoxy groups at the end of the epoxy chain are hydrophilic [45]. Therefore, fibers can form hydrogen bonds with the resin. As fibers are solid, hydrogen bonds can only form at the surface, not inside the fiber cell walls. The presence of nanofibrils increased the surface area of the cellulose fibers. The larger the surface area of the cellulose fibers, the more $-OH$ groups of cellulose react with the hydrophilic epoxy groups of the resin, Fig. 11. Consequently, the mechanical properties of the composites improved with the increasing number of nanofibrils on the microfibril surfaces. However, other types of interactions can occur between cellulose fibers and the epoxy resin,

such as electrostatic interactions, mechanical interlocking, and entanglement [43]. The thickness of the cellulose sheet and preparation method can also affect the mechanical strength of composite materials.

4. Conclusions

Alkali pretreatment (4, 8, and 12 cycles) followed by blending in an aqueous solution using a household blender was used to improve the fibrillation of OPEFB-derived cellulose fibers. The fiber diameter tended to become smaller and the diameter distribution narrower with increasing number of alkali pretreatment cycles. However, diameter distribution of the 8SB sample was wider than that of the 4SB sample. This was attributed to the continuous removal of the amorphous fraction of cellulose from the fibers, which contributed to fiber swelling, defibrillating, and breaking. The morphology, size, and dispersion of the reinforcing fibers were important parameters for evaluating the mechanical properties of cellulose-reinforced epoxy resin adhesive composites. The higher the content of thinner and homogenous fibers, the better the tensile properties of the composites. Blending cellulose in a mild (6 wt%) alkali solution required less energy than blending in an aqueous solution and improved the partial fibrillation of microfibrils to nanofibrils. The proposed pretreatment method can be used for partially deconstructing OPEFB microfibrils to prepare cellulose nanofibrils with high nanofibrillation and for engineering fiber-based materials and polymeric composites as reinforcements for thermosetting or thermoplastic resins.

Acknowledgments

The authors would like to thank Prof. Hitoshi Takagi and Dr. Antonio Norio Nakagaito (Tokushima University) and Prof. Rochmadi (Universitas Gadjah Mada) for helpful discussions. Funding: This work was supported by Ministry of Research, Technology and Higher Education,

Indonesia Government through the research grant of Penelitian Dosen Pemula (PDP) with the grant number of 081/SP2H/AMD/LT/DRPM/2020.

References

- [1] Shinoj S, Visvanathan R, Panigrahi S, Kochubabu M. Oil palm fiber (OPF) and its composites: a review. *Ind Crop Prod* 2011;33:7–22.
- [2] https://apps.fas.usda.gov/newgainapi/api/report/downloadreportbyfilename?filename=Oilseeds%20and%20Products%20Annual_Jakarta_Indonesia_3-15-2019.pdf.
- [3] Coseri S, Biliuta G, Simionescu BC, Stana-Kleinschek K, Ribitsch V, Harabagiu V. Oxidized cellulose-survey of the most recent achievements. *Carbohydr Polym* 2013;93:207–15.
- [4] Li L, Chen Y, Yu T, Wang N, Wang C, Wang H. Preparation of polylactic acid/TEMPO-oxidized bacterial cellulose nanocomposites for 3D printing via Pickering emulsion approach. *Compos Commun* 2019;16:162–7.
- [5] Lavoine N, Desloges I, Dufresne A, Bras J. Microfibrillated cellulose – its barrier properties and applications in cellulosic materials: a review. *Carbohydr Polym* 2012;90:735–64.
- [6] Ilyas R, Sapuan S, Atikah M, Asyraf M, Rafiqah SA, Aisyah H, Nurazzi NM, Norrahim M. Effect of hydrolysis time on the morphological, physical, chemical, and thermal behavior of sugar palm nanocrystalline cellulose (*Arenga pinnata* (Wurm.) Merr). *Textil Res J* 2021;91(1–2):152–67.
- [7] Abe K, Yano H. Comparison of the characteristics of cellulose microfibril aggregates of wood, rice straw and potato tuber. *Cellulose* 2009;16:1017–23.
- [8] Nakagaito AN, Takagi H. Easy cellulose nanofiber extraction from residue of agricultural crops. *Int J Mod Phys B* 2018;32:18400801–5.
- [9] Uetani K, Yano H. Nanofibrillation of wood pulp using a high-speed blender. *Biomacromolecules* 2011;12:348–53.
- [10] Kim JS, Lee YY, Kim TH. A review on alkaline pretreatment technology for bioconversion of lignocellulosic biomass. *Bioresour Technol* 2015;199:42–8. <https://doi.org/10.1016/j.biortech.2015.08.085>.
- [11] Dutra ED, Santos FA, Alencar BRA, Reis ALS, Souza RFR, Aquino KAS, Morais Jr MA, Menezes RSC. Alkaline hydrogen peroxide pretreatment of lignocellulosic biomass: status and perspectives. *Biomass Conv Bioref* 2018;8: 225–34.
- [12] Cai M, Takagi H, Nakagaito AN, Li Y, Waterhouse GIN. Effect of alkali treatment on interfacial bonding in abaca fiber-reinforced composites. *Compos Part A Appl Sci Manuf* 2016;90:589–97.
- [13] Sukmawan R, Saputri LH, Rochadi, Rochardjo HSB. The effects of the blending condition on the morphology, crystallinity, and thermal stability of cellulose microfibrils obtained from bagasse. *Indones J Chem* 2019;19:166–75.
- [14] Cai M, Takagi H, Nakagaito AN, Katoh M, Ueki T, Waterhouse ING, Li Y. Influence of alkali treatment on internal microstructure and tensile properties of abaca fibers. *Ind Crop Prod* 2015;65:27–35.
- [15] Scatolino MV, Bufalino L, Mendes LM, Guimarães Jr M, Tonoli GHD. Impact of nanofibrillation degree of eucalyptus and amazonian hardwood sawdust on physical properties of cellulose nanofibril films. *Wood Sci Technol* 2017;51: 1095–115.
- [16] Scatolino MV, Silva DW, Bufalino L, Tonoli GHD, Mendes LM. Influence of cellulose viscosity and residual lignin on water absorption of nanofibril films. *Procedia Eng* 2017;200:155–61.
- [17] Nechyporchuk O, Belgacem MN, Bras J. Production of cellulose nanofibrils: a review of recent advances. *Ind Crop Prod* 2016;93:2–25.
- [18] Chaker A, Alila S, Mutjé P, Vilar MR, Boufi S. Key role of the hemicellulose content and the cell morphology on the nanofibrillation effectiveness of cellulose pulps. *Cellulose* 2013;20:2863–75.
- [19] Sukmawan R, Wildan MW, Saputri LH, Rochmadi, Rochardjo HSB. Microfibrillated cellulose extraction from bagasse using a modified kitchen blender. *Mater Sci Forum* 2019;948:186–91.
- [20] Latip NA, Sofian AH, Ali MF, Ismail SN, Idris DMND. Structural and morphological studies on alkaline pre-treatment of oil palm empty fruit bunch (opefb) fiber for composite production. *Mater Today Proc* 2019;17:1105–11. <https://doi.org/10.1016/j.matpr.2019.06.529>.
- [21] Razak NWA, Kalam A. Effect of OPFB size on the mechanical properties and water absorption behaviour of OPEFB/PP nanoclay/PP Hybrid Composites. *Procedia Eng* 2012;41:1593–9.
- [22] Wu Y, Fei M, Chen T, Qiu R, Liu W. Biocomposites from bamboo fibers and palm oil-based thermosets: effects of natural phenolic cross-linkers. *Compos Commun* 2020;22:100489.
- [23] Wada W, Okano T. Localization of I α and I β phase in algal cellulose revealed by acid treatments. *Cellulose* 2001;8:183–8.
- [24] Popescu MC, Popescu CM, Lisa G, Sakata Y. Evaluation of morphological and chemical aspects of different wood species by spectroscopy and thermal methods. *J Mol Struct* 2011;988:65–72.
- [25] Kassab Z, Kassem I, Hannache H, Bouhfid R, Quais ALK, Achaby ME. Tomato plant residue as new renewable source for cellulose production: extraction of cellulose nanocrystals with different surface functionalities. *Cellulose* 2020;27:4287–303.
- [26] Oun AA, Rhim JW. Isolation of cellulose nanocrystals from grain straws and their use for the preparation of carboxymethyl cellulose-based nanocomposite films. *Carbohydr Polym* 2016;150:187–200.
- [27] Collazo-Bigliardi S, Ortega-Toro R, Chiralt Boix A. Isolation and characterisation of microcrystalline cellulose and cellulose nanocrystals from coffee husk and comparative study with rice husk. *Carbohydr Polym* 2018;191:205–15.
- [28] Kabir MM, Wang H, Lau KT, Cardona F. Chemical treatments on plant-based natural fibre reinforced polymer composites: an overview. *Compos B Eng* 2012;43: 2883–92.
- [29] Saba N, Tahir PM, Abdan K, Ibrahim NA. Preparation of fire-retardant nano-filler from oil palm empty fruit bunch fibers. *Bioresources* 2015;10:4530–43.
- [30] Nieves DC, Karimi K, Horváth IS. Improvement of biogas production from oil palm empty fruit bunches (OPFB). *Ind Crop Prod* 2011;34:1097–101.
- [31] Omrii MedA, Triki A, Guicha M, Ben Hassen Med, Arous M, El Hamzaoui HA, Bulou A. Effect of wool and thermo-binder fibers on adhesion of alfa fibers in polyester composite. *J Appl Phys* 2013;114:2241051–9. <https://doi.org/10.1063/1.4846215>.
- [32] Sun R, Fang JM, Goodwin A, Lawther JM, Bolton AJ. Fractionation and characterization of polysaccharides from abaca fibre. *Carbohydr Polym* 1998;37: 351–9.
- [33] Md Salim R, Asik J, Sarjadi MS. Chemical functional groups of extractives, cellulose and lignin extracted from native *Leucaena leucocephala* bark. *Wood Sci Technol* 2021;55:295–313.
- [34] Colom X, Carillo F, Nogués F, Garriga P. Structural analysis of photodegraded wood by means of FT-IR spectroscopy. *Polym Degrad Stabil* 2003;80:543–9.
- [35] Oh SY, Yoo DI, Shin Y, Seo G. Ftir analysis of cellulose treated with sodium hydroxide and carbon dioxide. *Carbohydr Res* 2005;340:417–28.
- [36] French AD. Idealized powder diffraction patterns for cellulose polymorphs. *Cellulose* 2014;21:885–96.
- [37] Kim UJ, Eom SH, Wada M. Thermal decomposition of native cellulose, Influence on crystallite size. *Polym Degrad Stabil* 2010;95:778–81.
- [38] Tonoli GHD, Holtman KM, Glenn G, Fonseca AS, Wood D, Williams T, Sa VA, Torres L, Klamczynski A, Orts WJ. Properties of cellulose micro/nanofibers obtained from eucalyptus pulp fiber treated with anaerobic digestate and high shear mixing. *Cellulose* 2016;23:1–18.
- [39] Siró I, Plackett D. Microfibrillated cellulose and new nanocomposite materials: a review. *Cellulose* 2010;17:459–94.
- [40] Sreekumar PA, Selvin P, Thomas, Saiter JM, Joseph K, Unnikrishnan G, Thomas S. Effect of fiber surface modification on the mechanical and water absorption characteristics of sisal/polyester composites fabricated by resin transfer molding. *Compos Part A Appl Sci Manuf* 2009;40:1777–84.
- [41] Gassan J, Bledzki AK. Possibilities for Improving the mechanical properties of jute/epoxy composites by alkali treatment of fibres. *Compos Sci Technol* 1999;59: 1303–9.
- [42] John MJ, Anandjiwala RD. Recent developments in chemical modification and characterization of natural fiber-reinforced composites. *Poly Compos* 2008;29: 187–207.
- [43] Dilamian M, Noroozi BA. Combined homogenization-high intensity ultrasonication process for individualization of cellulose micro-nano fibers from rice straw. *Cellulose* 2019;26:5831–49.
- [44] Akpan EI, Shen X, Wetzel B, Friedrich K. 2 - design and synthesis of polymer nanocomposites. In: Pielichowski K, Majka TM, editors. *In micro and nano technologies, polymer composites with functionalized nanoparticles*. Elsevier; 2019. p. 47–83.
- [45] Massingill JL, Bauer RS. Epoxy resins. In: Craver CD, Carraher CE, editors. *Applied polymer science: 21st century*. Pergamon; 2000. p. 393–424.